Received: 25 March 2019 | Revised: 27 November 2019 | Accepted: 29 November 2019 | Published on: 18 December 2019

DOI: 10.1002/met.1868

RESEARCH ARTICLE

Meteorological Applications RMetS

Application of a simple analytical model to severe winds produced by a bow echo like storm in northeast Italy

Arturo Pucillo[1] | **Mario M. Miglietta**[2] | **Kelly Lombardo**[3] | **Agostino Manzato**[1,2]

[1]OSMER ARPA FVG, Palmanova, Italy

[2]Consiglio Nazionale delle Ricerche, Istituto di Scienze dell'Atmosfera e del clima, Padua, Italy

[3]Department of Meteorology and Atmospheric Science, Pennsylvania State University, University Park, Pennsylvania, USA

Correspondence
Arturo Pucillo, OSMER ARPA FVG, Via Natisone 43, Palmanova, UD 33057, Italy.
Email: arturo.pucillo@meteo.fvg.it

Abstract

A strong mesoscale convective system affected northeastern Italy on August 8, 2008. Notable damage and two casualties resulted, mainly due to the strong wind gusts. The event is analysed using observations, including surface data from a meso-network of meteorological stations, radar reflectivity and velocity data from a C-band Doppler radar, polar satellite images, lightning measurements from a lightning detection network and the ambient thermodynamic conditions derived from local radiosoundings. The role of the cold front is investigated; in particular, the associated strong wind descending from the Alps, which interacted with the preexisting convection in the plain, is analysed to understand the way it affected the storm development. A simple density current model is applied to describe the flow characteristics and to identify the mechanisms that could support the development of such a high wind speed. Lastly, observed wind speeds are compared with the theoretical estimates from the proposed model. The results show that different factors contribute to the very strong wind gusts registered by surface stations. The main contributor to the windstorm is a density current (a) driven by the cold front, (b) maintained by the interaction between the cold air impinging on the Friuli Venezia Giulia plain from the north and the strong regional density gradient and (c) eventually enhanced by the storm cold pool. This study highlights the complex evolution of severe storms in a region on the lee side of the Alpine chain, and emphasizes the role of the orography in the enhancement of storm.

KEYWORDS

bow echo, density current, gust, thunderstorm, wind

1 | INTRODUCTION

Each year, a few severe weather events occur in northeast Italy, a region confined by the Alps on its northern border and by the warm Adriatic Sea on its southern border. A high frequency of storms has been reported, particularly during the warm season, including frequent occurrence of severe events like tornadoes, hailstorms and lightning (Giaiotti *et al*., 2007; Pucillo *et al*., 2009; Manzato, 2012; Feudale and Manzato, 2014). In general the area is one of the most affected by heavy rain and thunderstorms over the whole of Europe (Isotta *et al*., 2014; Poelman *et al*., 2016; Pavan *et al*., 2019; Taszarek *et al*., 2019a). In particular, severe events have been

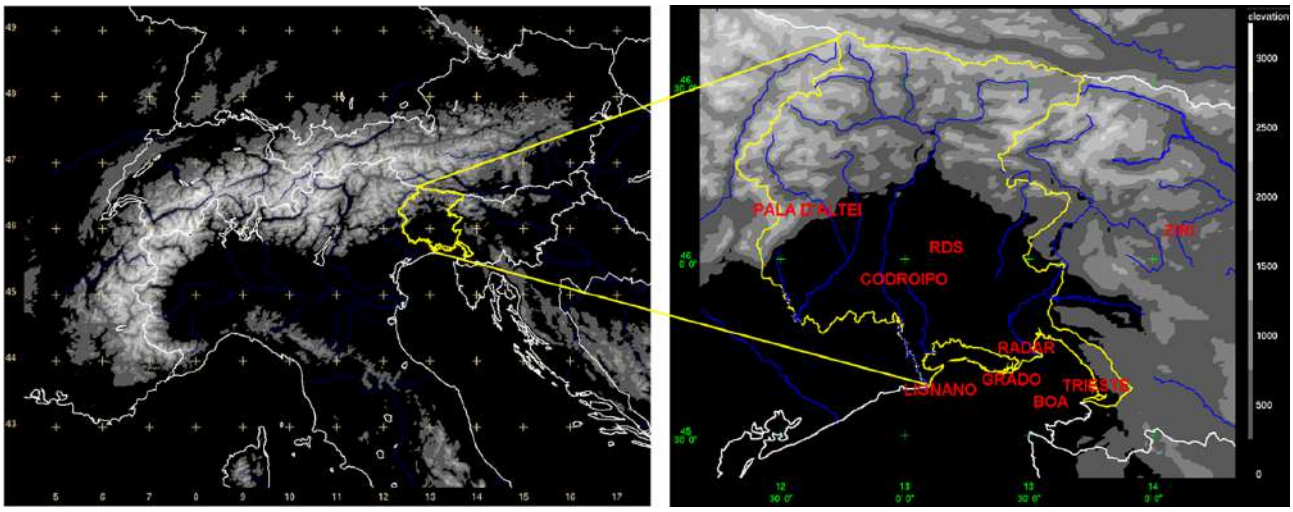

FIGURE 1 Studied area map. On the left the position of Friuli Venezia Giulia region in the northern Italy–central Europe area. On the right, Friuli Venezia Giulia borders, orography, main rivers and labels of the Regional Meteorological Observatory (OSMER) meteorological stations considered in this study. The positions of the 16044 radiosounding base of Campoformido and the OSMER radar in Fossalon di Grado are marked (RDS and RADAR respectively). The position of Žiri town in Slovenia, hit by big hailstones, is also shown

observed and studied in the region of the Friuli Venezia Giulia (FVG) plain (Figure 1) over the last 20 years (Bechini *et al*., 2001; Giaiotti *et al*., 2001; Bertato *et al*., 2003; Manzato *et al*., 2015). High impacts from such phenomena have been recognized as a danger to human safety and recreational and commercial activities, making short range forecasts and warnings critical for civil protection purposes (Miglietta *et al*., 2016). Previous studies have indicated that potential instability is a main player supporting the development of severe thunderstorms in that area (Manzato, 2007; Pucillo and Manzato, 2013). Even a small increase in sea surface temperature of the Adriatic Sea may produce additional low-tropospheric vapour via evaporation, thus providing an environment richer in moisture, increasing low-level equivalent potential temperature (θ_e), and potential instability (Miglietta *et al*., 2017). Nevertheless, the mesoscale and storm-scale dynamics and the interaction between storms and the regional topography during these severe weather events are still poorly understood (Davolio *et al*., 2016).

This research focuses on an event that impacted FVG in the late evening of August 8, 2008, mainly characterized by severe winds near the surface. It is hypothesized that the terrain conformation contributed to an increase in surface wind speed, which aided in the organization and intensification of existing convective cells into a bow echo type storm and the subsequent development of damaging winds along the path.

The observed damage, which was attributed to linear winds, contrasted with the presence of funnel clouds (with suspected touchdown), reported (and photographed) during the early stage of the storm, so that the

FIGURE 2 Photos of damage reported in the Grado camping site. The parallel trees pulled down suggest linear winds instead of tornadic winds. Arrows indicate the position and direction of fallen trees

description and classification of the storm was initially uncertain. The worst damage was due to straight line winds, affecting in particular the Al Bosco campground, along the coast, near the town of Grado. Two casualties occurred due to fallen trees on the camping structures (Figure 2). Funnels and waterspouts were reported by spotters and local media over an area about 15–20 km east of Grado before the passage of the storm, which motivated the media to attribute the damage to a "tornado." Nevertheless, the results of the present analysis reveal storm morphological elements similar to a bow echo mesoscale convective system (Wakimoto *et al*., 2006), although the features have smaller space–time scales compared to those reported in the literature.

A set of temporally high resolution observations (5 min meteorological surface data, 5 min radar data, 5 min satellite data and 1 s lightning data) is used to detail the evolution of the event, and to compare it with a simple conceptual model. Analyses are performed to identify the mechanisms that support the straight line winds during this bow echo like event.

The paper is organized as follows. Section 2 provides a general overview of the observational tools, such as the available data and instrumentation characteristics. In Section 3, a synoptic and mesoscale analysis of the event, measurements of wind speed/direction, pressure and equivalent potential temperature of the station meso-network managed by the Regional Meteorological Observatory of the Regional Agency for Environment Protection of the FVG region (OSMER ARPA FVG) are discussed. Moreover, time series of meteorological observations at several ground stations are provided. A simple dynamic model for estimation of the surface flow, based on the momentum equation, is implemented to establish the relationship between the measured horizontal pressure gradient and the observed wind speed, and to discriminate between the contributions to the flow due to the different terms in the equation. Lastly, a characterization of the Froude number associated with the low-level flow is provided. Section 5 provides concluding remarks.

2 | DATA AND METHODS

Wind speed and direction are provided by a network of 39 anemometers placed at a height of 10 m above ground level and located all over the FVG region (Figure 1). The instruments are magnetic induction anemometers with a three-cup whirl, built by SIAP-MICROS Company. The precision in wind magnitude is 0.25 $m \cdot s^{-1}$ decreasing to 0.7 $m \cdot s^{-1}$ for wind magnitudes exceeding 20 $m \cdot s^{-1}$; precision in wind direction is 0.5%. Pressure measurements are provided by electronic sensors placed 1.8 m above ground, with a resolution of 0.1 hPa. Temperature and relative humidity are measured by electronic sensors with 0.1°C and 1% resolution, respectively. Station data are available every 5 min. For wind, 5 min values are computed as the average of measurements over 1 min, while hourly gusts are the peaks registered by sampling every 10 s.

Vertical maximum intensity (VMI) reflectivity and Doppler winds are estimated from the Galileo GPM-500C Fossalon di Grado C-band dual-polarization Doppler radar (location shown in Figure 1), which, at that time, provided a full volume scan every 5 min. For wind speeds greater than 16 $m \cdot s^{-1}$, the Doppler velocity is affected by range folding, due to the operational setting of the instrument, which is limited to ± 16 $m \cdot s^{-1}$.

Atmospheric instability indices are calculated through the Python software called Sound_Analys.py (Manzato and Morgan Jr, 2003) from the high vertical resolution radiosoundings released by the Italian Air Force (Aeronautica Militare) at the Udine Campoformido base (World Meteorological Organization code 16044, 46.04 ° N, 13.19 ° E coordinates, identified as "RDS" in Figure 1), using a Vaisala RS-92 rawinsonde. The Udine sounding base provided four launches per day until February 2006 but, after that date, the 0600 UTC and 1800 UTC radiosonde launches were mostly discontinued. During the period studied here, the 0600 UTC sounding profile was still available. A Thetaplot diagram (Morgan Jr, 1992; Manzato and Morgan Jr, 2003) is implemented to plot the atmospheric vertical profile. Equivalent potential temperature calculations are derived using the Bolton (1980) approximation.

Real time satellite imagery is provided by Eumetsat Meteosat Second Generation data. The 10.8 μm IR (channel 9) and high-resolution VISIBLE (channel 12) are most often used by the OSMER ARPA FVG forecasting service but are not shown in the present analysis since a false colour composite image derived from the moderate resolution imaging spectroradiometer (MODIS) instrument (on board the NASA AQUA polar satellite) is analysed here. Lightning data are provided by the CESI-SIRF archive (more information at http://www.fulmini.it) through a ground-based lightning detection network using Vaisala sensors (Poelman *et al*., 2016) measuring, at that time, only the cloud-to-ground strikes.

3 | METEOROLOGICAL ANALYSIS

3.1 | Synoptic analysis

After a long period characterized by a quasi-stationary anticyclonic ridge over the central Mediterranean Sea that led to anomalously high air and sea temperatures in the FVG area, a trough approached Western Europe from the Atlantic Ocean on August 6, 2008. A baroclinic short wave within the larger trough moved southeastward, from Great Britain towards the Adriatic Sea, moving over northeastern Italy by August 9 (Figure 3a) and inducing surface pressure to fall (Figure 3b). The associated cold front approached the Alps on August 7, 2008 and was preceded by a warm and moist southwesterly flow above 800 hPa in a potentially unstable environment (see Section 3.2 for a discussion of the soundings shown in Figure 4).

The interaction between the cold front and the Alpine orography caused a leeside cyclogenesis (the so-called Genoa Low, Figure 3b) due to a typical mechanism of front-across-the-Alps pattern evolution (Buzzi and Tibaldi, 1978; McGinley, 1982; Steinacker, 1984). During

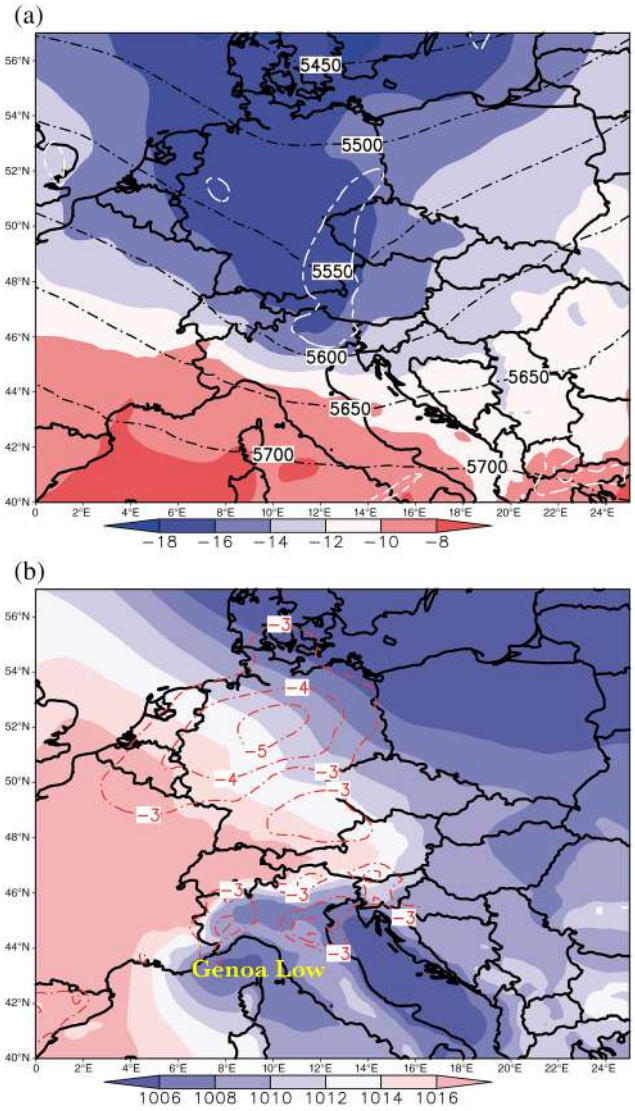

FIGURE 3 Analysis map based on the European Centre for Medium-Range Weather Forecasts model, at 0000 UTC on August 9, 2008, displaying (a) the geopotential height in metres (black dash-dot lines), temperature in °C (shaded) and potential vorticity at 500 hPa (white dashed contours at 1.5 potential vorticity units); and the (b) mean sea level pressure (shaded) and pressure tendency (red dash-dot contour, plotted only where exceeding −3 hPa/6 hr). The "Genoa Low" depression position is also indicated. [Correction added on 06 January 2020, after first online publication: The sub-figure b was previously missing and has been added in this current version.]

August 8 daytime, the right-exit region of an intense 300 hPa southwesterly jet streak, located behind the front, moved over northern Italy, with upper-level divergence on its leading left edge over the eastern Alpine region (not shown). This feature was superposed on southerly winds near the surface, associated with the surface low cyclonic circulation.

As a consequence, vertical wind shear occurred in the region and was favourable for the upscale growth of isolated cells evolving into supercells and clustering into a mesoscale convective system. In fact, between 1100 and 1300 UTC of August 8, 2008, large hailstones were produced during a severe hailstorm, while the windstorm developed after 1900 UTC. Subsequently, during the evening, the passage of the cold front through the FVG area was associated with the transition of low-level wind from northwesterly to northeasterly; meanwhile, an anticyclonic ridge, located to the west of the trough, pushed into the region, rotating the upper-level winds from the northwest.

3.2 | Mesoscale analysis and instability

In this section, a brief analysis of the soundings launched at Udine Campoformido at 0600 UTC (not shown) and at 1200 UTC (Figure 4) is presented in order to depict the evolution of the instability conditions that supported this event.

At the time of convective initiation, the troposphere was potentially unstable because of a layer of high equivalent potential temperature θ_e, of around 338 K in the lowest 1,000 m, already present at the time of the sounding launch (1143 UTC, Figure 4). Using the 30 hPa thick mixed most unstable parcel (MUP) in the lowest 250 hPa as the initial parcel, with the virtual correction implemented by the Tv scheme of Manzato and Morgan Jr (2003), the convective available potential energy (CAPE) was 1,730 $J \cdot kg^{-1}$. Notable values of DT500 (also called the most unstable lifted index, MULI), calculated as the temperature difference at 500 hPa between the lifted MUP and the environmental temperature, were present (−6.8°C).

The hodograph and vertical wind profile illustrate the presence of significant vertical shear. The observed 11.8 $m \cdot s^{-1}$ of bulk shear between the surface and 850 hPa winds was near the 95th percentile of the distribution for Udine soundings (considering a sample of all cases in the thunderstorm season, April–November, in the years 1995–2007; Manzato and Morgan Jr, 2003) and was mainly due to veering in the lowest 2.5 km. A 163.5 $J \cdot kg^{-1}$ value of 0–3 km storm relative helicity has been computed, that describes an environment typical for rightmoving supercells.

The sounding 6 hr earlier (not shown) showed an even more unstable environment (CAPE = 2,790 $J \cdot kg^{-1}$ and MULI = −8.8°C respectively). However, the very high θ_e of its initial MUP was partly due to a nearly saturated low-level layer that was probably affected by pre-existing convective clouds. The morning convection activity was so intense that the 1200 UTC sounding (launched at 1100 UTC) probably crashed passing near a storm. Hence, a new sounding was launched at 1143 UTC; as an effect of the storm activity, the atmosphere

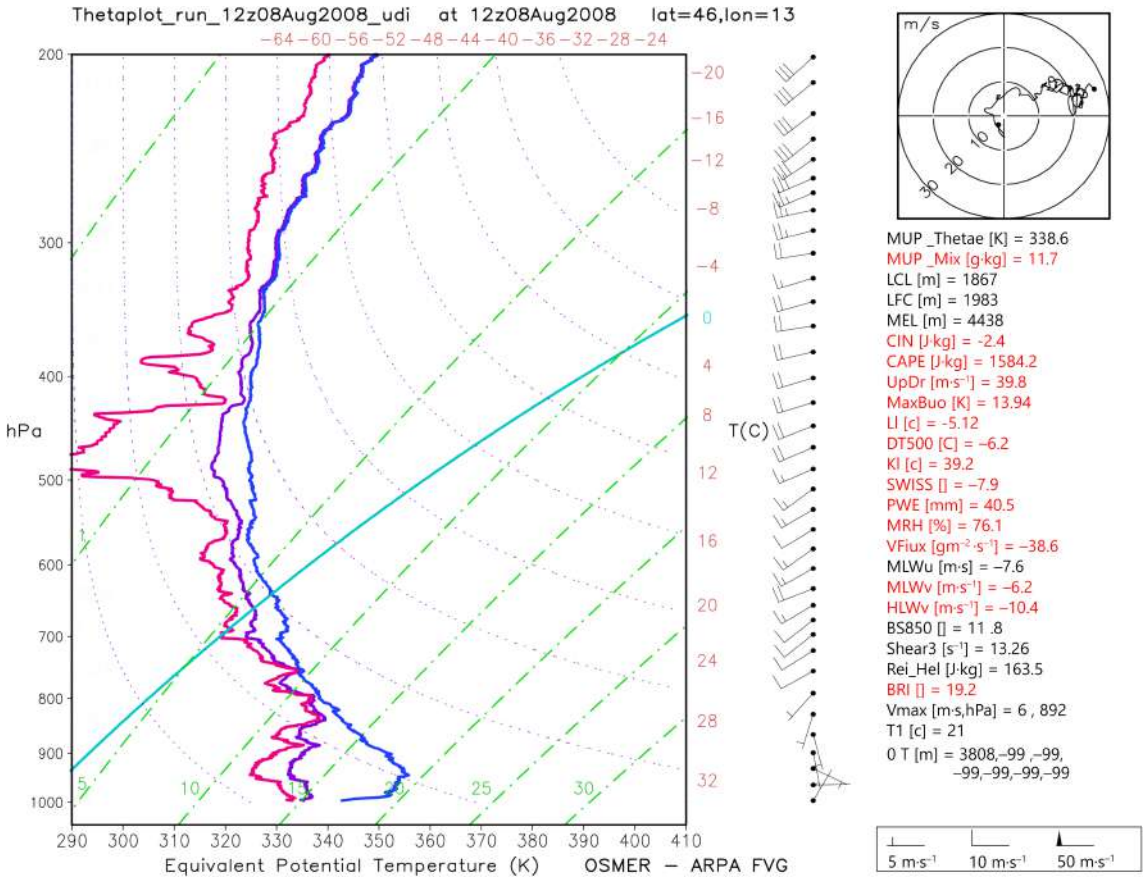

FIGURE 4 Thetaplot diagram of the former 16044 radiosounding at 1200 UTC on August 8, 2008, with indication of the hodograph and some derived instability indices. Thin left-slanted curves are the isotherms that intersect the temperature values on the thick right line (which is the saturated equivalent potential temperature, θ_{es}, profile), the wet bulb temperature on the thick middle line (equivalent potential temperature, θ_e) and the dew-point temperature on the thick left line (dew-point equivalent potential temperature, θ_{ed}). See Morgan Jr (1992) and Manzato and Morgan Jr (2003) for more details

FIGURE 5 Hailstones collected in Žiri (Slovenia) during the afternoon (Neva Pristov, personal communication)

was slightly drier and cooler than that at 0600 UTC. Even if none of these soundings can be defined as completely "uncontaminated" by cloud presence (as the lifted parcel theory requires), the potential instability of the atmosphere during the morning and afternoon of August 8, 2008 was particularly high, contributing to the formation of widespread and severe hailstorms between 1100 and 1300 UTC. At that time severe hail damaged a hospital in Latisana (about 10 km northnorthwest of Lignano; Figure 1). During the afternoon hailstones up to 5 cm in diameter (Figure 5; personal communication of Neva Pristov, Environmental Agency of the Republic of Slovenia) were reported at Žiri in Slovenia, about 40 km east of the FVG border.

During the late hours of August 8 potential instability was reduced as a consequence of a θ_e decrease in the low levels, due to both the passage of the cold front and the diabatically cooled air from previous storms.

3.3 | Evolution of evening convection

After 2000 UTC, the advection of cold and dry air behind the front resulted in a sudden increase of the surface

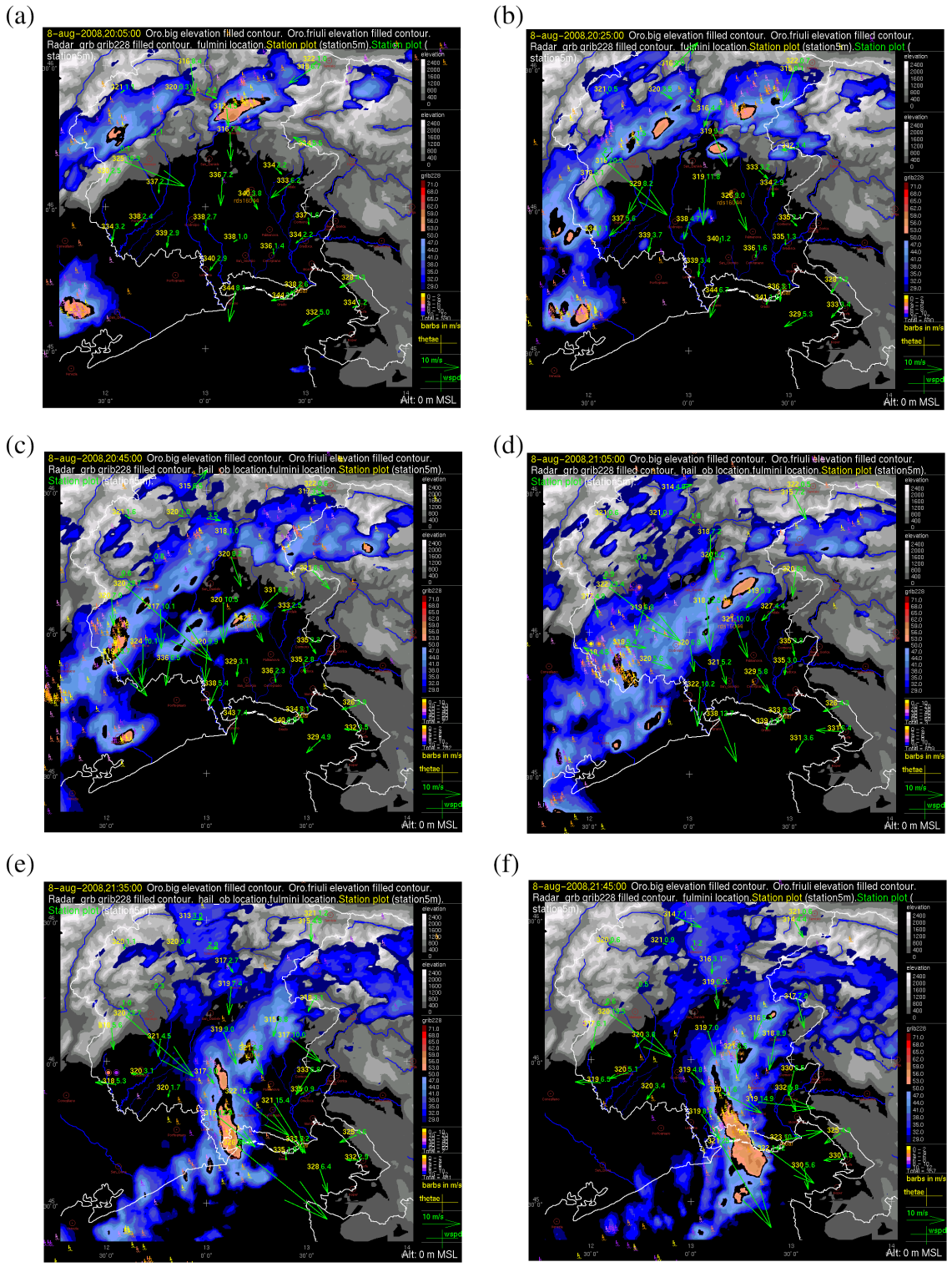

FIGURE 6 Panels of the National Center for Atmospheric Research (USA) visualization tool called Zebra (Corbet *et al.*, 1994) showing meteorological station data (wind vectors, wind speed [$m \cdot s^{-1}$] and equivalent potential temperature [K]), cloud-to-ground lightning (reported as little flashes) and radar vertical maximum intensity (VMI) shaded contours of the Regional Meteorological Observatory radar. Nominal time refers to 2005 UTC for (a), 2025 UTC for (b), 2045 UTC for (c), 2105 UTC for (d), 2135 UTC for (e), 2145 UTC for (f). Station data are 5 min data observed at the nominal time. VMI radar data are centred 5 min before the nominal time. Lightning data were collected in the last 12 min before nominal time. There is the presence of some hail-pad hits in the last hour before nominal time on the western part of the plain, in the early stage of the convective event, marked as little circles on the map

northwesterly wind that interacted with the preexisting convective cells at the foot of the Alps, over the plains of FVG and Veneto (the adjacent Italian region at the western border of FVG). It is hypothesized that the increase in low-level winds contributed to the growth in organization and intensity of the convective cells up to bow echo like level and to the associated damaging winds within the path of the gust front. Subsequently, surface winds were further enhanced by the development of a leeside cyclone that interacted with the cold front driven flow, as discussed later.

Between 2005 and 2025 UTC, a quasi-stationary line of convective cells was over the Alps, associated with the incoming cold front, whereas a separate thunderstorm which developed in the afternoon still persisted in the coastal regions to the southwest of the region (Figure 6a, b). At this time, an intense northwesterly wind was observed at the Pala d'Altei station (1,528 m above mean sea level), while high θ_e values (334–344 K) were still present on the FVG plain.

Between 2045 and 2105 UTC, the thunderstorms over the western part of the region intensified, while the cold pool, associated with the afternoon storms over the Alps, was advected by northwesterly winds toward the high plains (Figure 6c,d), producing an additional θ_e drop of about 20 K in that area. Between 2135 and 2145 UTC, the thunderstorm line over the Alps moved towards the FVG plain, "merging" with the weaker preexisting convective cells at the foothills and near the coast (Figure 6e,f). The θ_e inland decreased below 320 K due to the wide storm outflow, whereas higher values (up to 338 K) were still present near the coastline. Winds were northnorthwesterly at all locations except for the Trieste area (southeastern part of FVG), where the leeside cyclone driven northeasterly winds prevailed.

Analysing the pattern of θ_e in more depth, two different intrusions of dry air near the surface are shown (Figure 7). The first occurred at 2015 UTC (Figure 7a), driven by a northerly wind flowing out of the Tagliamento Valley, near Gemona town (about 30 km north of RDS in Figure 1), associated with the outflow of a thunderstorm in the mountain area (Figures 6a,b). The second was triggered 30 min later by the northwesterly flow originating near Pala D'Altei (Figure 7b). As noted by OSMER ARPA FVG forecasters (personal communication), this feature is typical of cold fronts coming from the northwest: storms often develop or enhance in the plain or in the coastal area of FVG 1 or 2 hr after the increase in dry northwesterly wind at the Pala d'Altei station. By 2135 UTC, the extension of the area of maximum θ_e reduced, whereas the convective system transitioned into a bow echo like system and moved southeastward toward the coast (not shown).

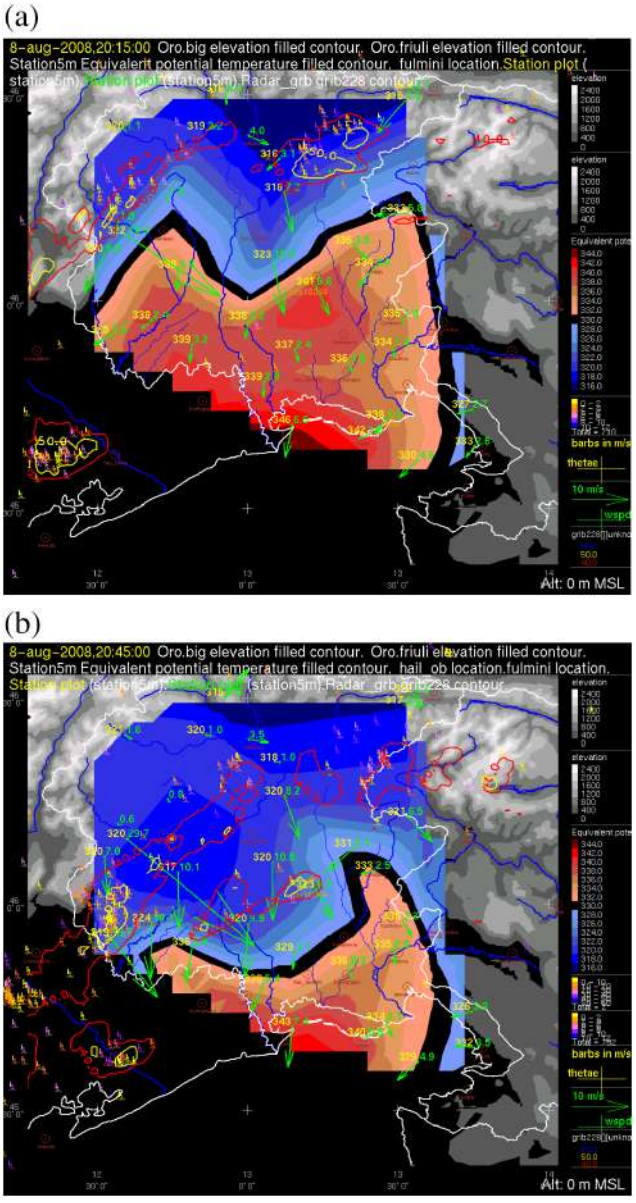

FIGURE 7 As Figure 6 but the equivalent potential temperature is spatialized and shaded, at two different times: (a) 2015 UTC, (b) 2045 UTC. The vertical maximum intensity is represented as solid contour lines (red at 40 dBZ, yellow at 45 dBZ)

Figure 8 shows an enhanced RGB elaboration of the brightness temperature of band 31 (10.78–11.28 μm) of the MODIS Aqua polar orbiting satellite, with a horizontal resolution of about 500 m (Figure 8, courtesy of Martin Setvak, Czech Hydrometeorological Institute). At the time of the frame, 2105 UTC, the convective system was just before the development into a bow echo like structure in the radar signature (Figure 9), with a core storm characterized by low brightness temperature values (near 213 K, i.e. −60°C), i.e. having a very cold top.

The convective system resembles a bow echo storm (e.g. VMI in Figure 6e), whose shape is similar to that

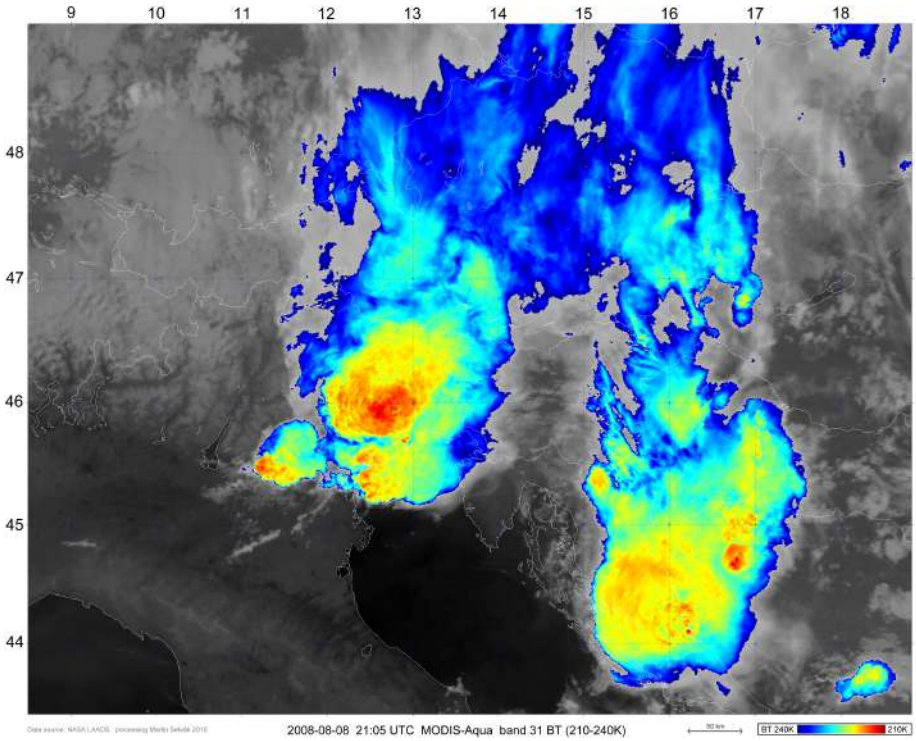

FIGURE 8 RGB composition of the brightness temperature of band 31 of the MODIS Aqua polar orbiting satellite with horizontal resolution of 500 m centred at 2105 UTC in the northeastern Italy area (courtesy of Martin Setvak, Czech Hydrometeorological Institute)

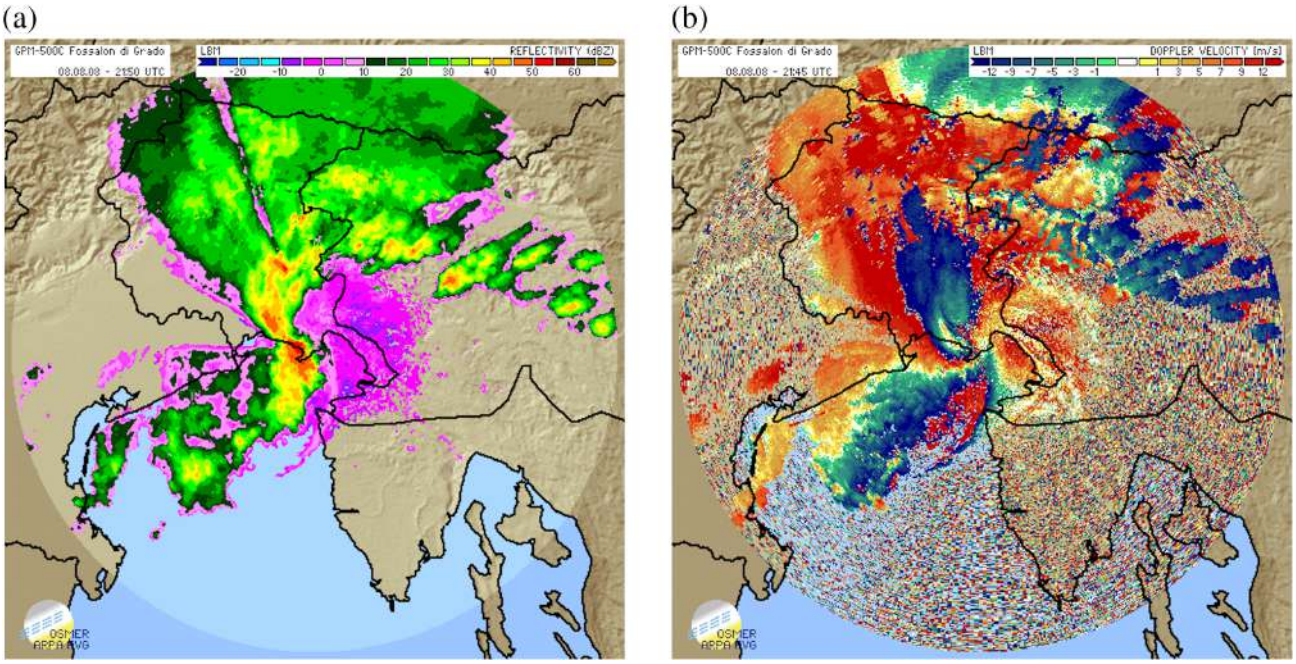

FIGURE 9 (a) Vertical maximum intensity (VMI) and (b) Doppler velocity at 2150 UTC. The Doppler signatures show evidence of multiple folding due to the strength of the winds and the setting of the radar (positive velocities refer to incoming winds, i.e. opposite to the usual convection). In both VMI and Doppler, the signature of the gust front is just in front of the main echo of the storm. [Correction added on 06 January 2020, after first online publication: Figures 9 and 10 were mistakenly interchanged and have been updated in this current version.]

reported by Miglietta *et al.* (2016) and in fig. 5d of Manzato *et al.* (2015) in the same area, but the temporal and spatial scales are relatively small compared to bow echo studies, as documented in the literature (e.g. Weisman, 1993). Therefore, it could be classified between the bow echo and the quasi-linear convective system that is characterized as a type of mesoscale convective system with a contiguous or nearly contiguous chain of convective echoes, with radar reflectivity values greater than 35 dBZ, organized into a linear or curved leading line. These storms typically

have a length scale of 50–100 km, an aspect ratio of 5:1,and temporal duration longer than or equal to 3 hr (e.g. Bluestein and Jain, 1985; Parker and Johnson, 2000; Coniglio *et al.*, 2007; Lombardo and Colle, 2010; Lombardo and Colle, 2012). While these and other bow-shaped systems may exhibit bookend vortices and severe surface winds, they do not exhibit an elevated rear inflow at the leading edge of the system, unlike the "true" bow echo storms (Weisman, 1993; George and Knievel, 2006).

In the event under study, rapid storm development (of the order of a few minutes), high VMI values (Figure 9a) and high wind speeds in the lower troposphere (Figure 9b) suggest that the cold flow moving down from the Alps, driven by the cold front, played a major role in enhancing storm severity and served as a bow echo rear inflow jet that, otherwise, is typically generated through internal storm dynamics (e.g. Weisman, 1993). Furthermore, the cold air advection moving down the Alps acted as a forced rear inflow jet and caused (and/or accelerated) the transition of a single/multicell storm into a bow echo like storm, although with smaller space–time characteristics, as explained above.

Although the Fossalon radar image at that time was partially corrupted, radar reflectivity shows that at 2150 UTC the system reached the town of Grado (Figure 9a), where the worst damage and two casualties occurred. These are the last data available before the Fossalon radar entered auto-protection mode due to the notable wind intensity. The wind speeds measured by OSMER ARPA FVG surface stations (45 $m \cdot s^{-1}$) and the Doppler signatures (Figure 9b) agree with other well documented bow echo events (see Atkins *et al.*, 2005, and references therein).

Subsequently, the main convective system moved eastward following the coastline and caused damage in the Duino area, north of Trieste. A storm chaser (Marko Korosec, www.weather-photos.net) photographed a waterspout over the Sistiana Bay, between Duino and Grado. Moreover, people watching the storm from Trieste harbour informed the media that, some minutes before the arrival of the gust, lightning flashes revealed a waterspout several miles to the northwest, in the direction of Grado, that probably inspired the media to misclassify this storm as a "tornadic event."

The presence of an observed waterspout in the advancing edge of the main storm (as recently observed for two waterspouts in northwestern Italy; Miglietta *et al.*, 2019) indicates the possibility of another mechanism able to produce such damaging winds. French and Parker (2014) and Taszarek *et al.* (2019b) describe simulated and observed cases respectively of moving squall lines that reach preexisting supercells, merge with them and provide a trigger to the downward transfer of an enhanced rear inflow jet. The simulated case (French and Parker, 2014) shows that the merging between squall lines and supercell is discriminant for reaching such damaging intensities. In our case, the presence of a supercell in the convective cluster at the foothills at

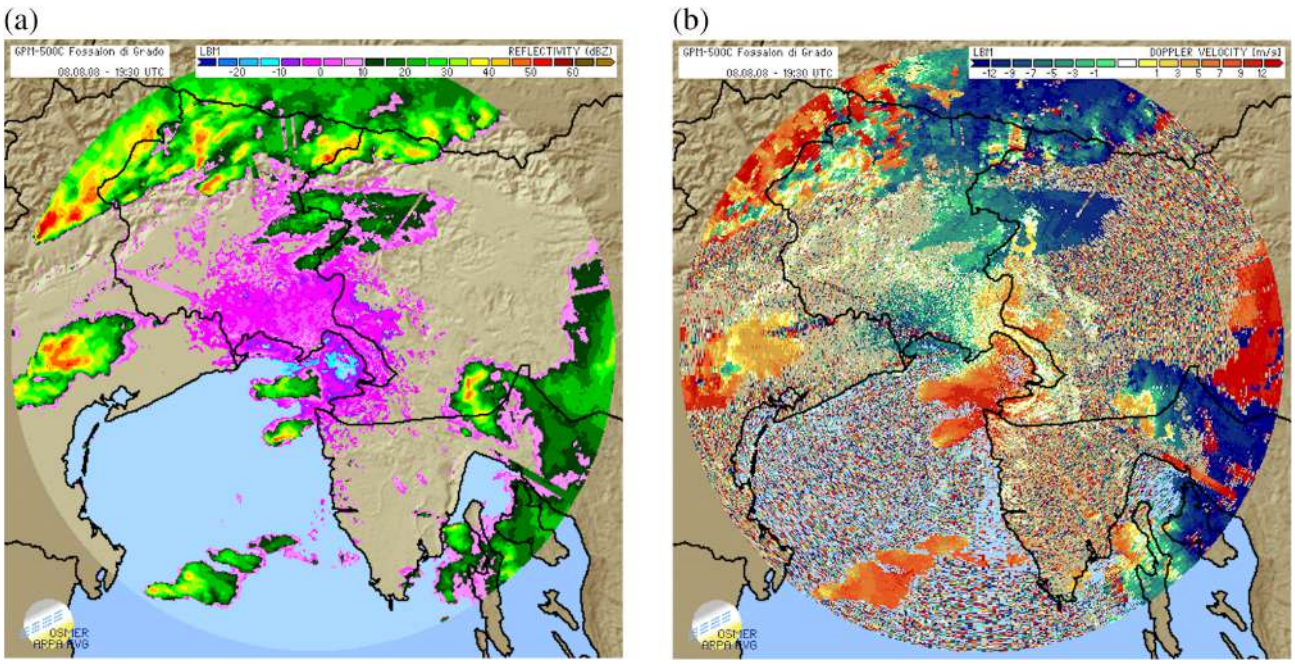

FIGURE 10 (a) Vertical maximum intensity (VMI) and (b) Doppler velocity at 1930 UTC. Doppler signatures show a possible signal of opposite radial velocities in the black circled area, associated with a cluster of high VMI. [Correction added on 06 January 2020, after first online publication: Figures 9 and 10 were mistakenly interchanged and have been updated in this current version.]

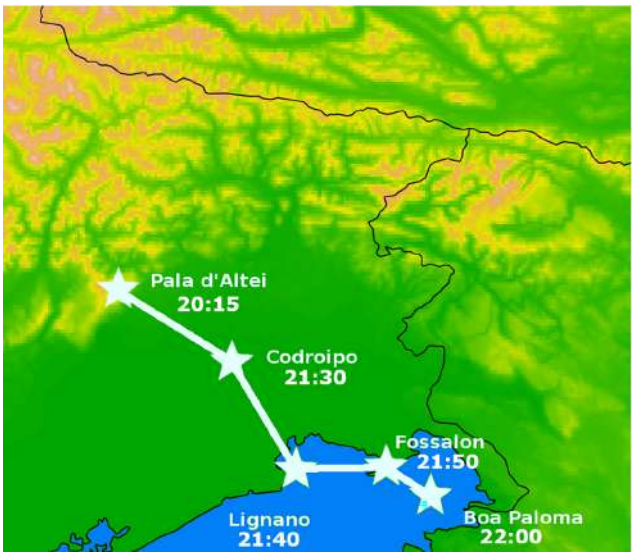

FIGURE 11 Ideal trajectory of the storm following the stations involved in the time series in the following figure, Figure 12, with indication of times. Stars in the figure represent the position of meteorological stations. Friuli Venezia Giulia region borders are marked by a black line

around 1930 UTC (i.e. about 1 hr before the squall line enters the FVG plain and merges with preexisting convection) is possible but cannot be demonstrated beyond doubt. The Doppler radar lowest beam scan, shown in Figure 10b, shows a possible mesocyclone in a restricted area of opposite radial velocities, associated with a cluster of VMI higher than 50 dBZ (Figure 10a). However, this feature disappears after only 10 min (not shown), possibly due also to limitations in Doppler radar scanning (the lowest beam composite image is affected by sharp gradients in velocity when the system approaches the radar site location). Hence, the absence of a mesocyclone signature in the further radar scans cannot support "supercell-based" interpretation in a more convincing way.

3.4 | Time series analysis

The movement of the bow echo like storm over the region is represented in Figure 11, while Figure 12 shows the time series of surface pressure, wind and θ_e, measured by some of the OSMER ARPA FVG meteorological stations. The stations chosen are located on an ideal strip along the trajectory of the main convective event, i.e. from Pala d'Altei (Prealpi Carniche ridge, at 1,528 m above mean sea level), to Codroipo (western plain) and to Boa Paloma (sea).

At about 2000 UTC, cold and dense air associated with the cold front reached the pre-Alpine ridge, as visible in the time series in Pala d'Altei station, located within the Alps (Figure 12a). A 14 K drop in θ_e occurred in less than 20 min (from 332 K to 318 K). Simultaneously, the pressure decreased by 5 hPa, reaching its minimum value 25 min after the minimum in θ_e. This cold advection is well correlated with the onset of a strong (30 $m \cdot s^{-1}$) northwesterly wind, as shown in the wind time series.

At Codroipo station, located 35 km south of the mountain ridge within the FVG plain, the decrease in θ_e started 20 min after the drop at Pala d'Altei (2020 UTC) and was associated with moderate northeasterly winds (6–9 $m \cdot s^{-1}$), with only a slight change in pressure (Figure 12b). This is the signature of the cold air moving south from the Tagliamento Valley, which may have helped to initiate convection within the FVG plain, as shown in the radar VMI (Figure 6c). Subsequently, the surface pressure rose between 2100 and 2200 UTC, associated with the outflow from the convective precipitation. This behaviour is in theoretical agreement with the passage of a gravity wave associated with the gust front.

Following Haertel *et al.* (2001), gravity current outflow associated with mass advection can be distinguished from gravity wave propagation associated with mass convergence, with a continuous transition stage between these two extreme kinds of behaviour. Thus, the pressure rise between 2100 and 2130 UTC is coherent with the gravity wave mechanism, since it corresponds to a change in surface wind but little or no change in surface temperature (keeping in mind that the first temperature drop had already occurred before). One of the conditions in Haertel *et al.* (2001) for the distinction of the two categories is the depth of the cool tropospheric layer, which in the case of the Pala D'Altei station can be assumed to be higher than 1.5 km because the time series in Figure 12a provides observations at an altitude of more than 1,500 m above mean sea level.

However, different outflow characteristics, as underlined in the following analysis, can be observed during the evolution of this storm. Note that the Codroipo station was not perfectly along the path of the storm core, which passed farther south; thus, the effect of the storm was smaller there, compared to other stations. The recovery from this pressure rise corresponds to the onset of the northeasterly synoptic wind, almost 2 hr later.

The time evolution in Lignano station (western coastal station) is similar to that in Codroipo (Figure 12c). A decrease in θ_e, at about 2100 UTC, accompanied the arrival of a northwesterly wind. However, the pressure rise occurred more suddenly than at Codroipo, at 2120 UTC, when the gust front associated with convection moved over the station. The strong northwesterly wind followed the passage of the storm for about 1 hr,

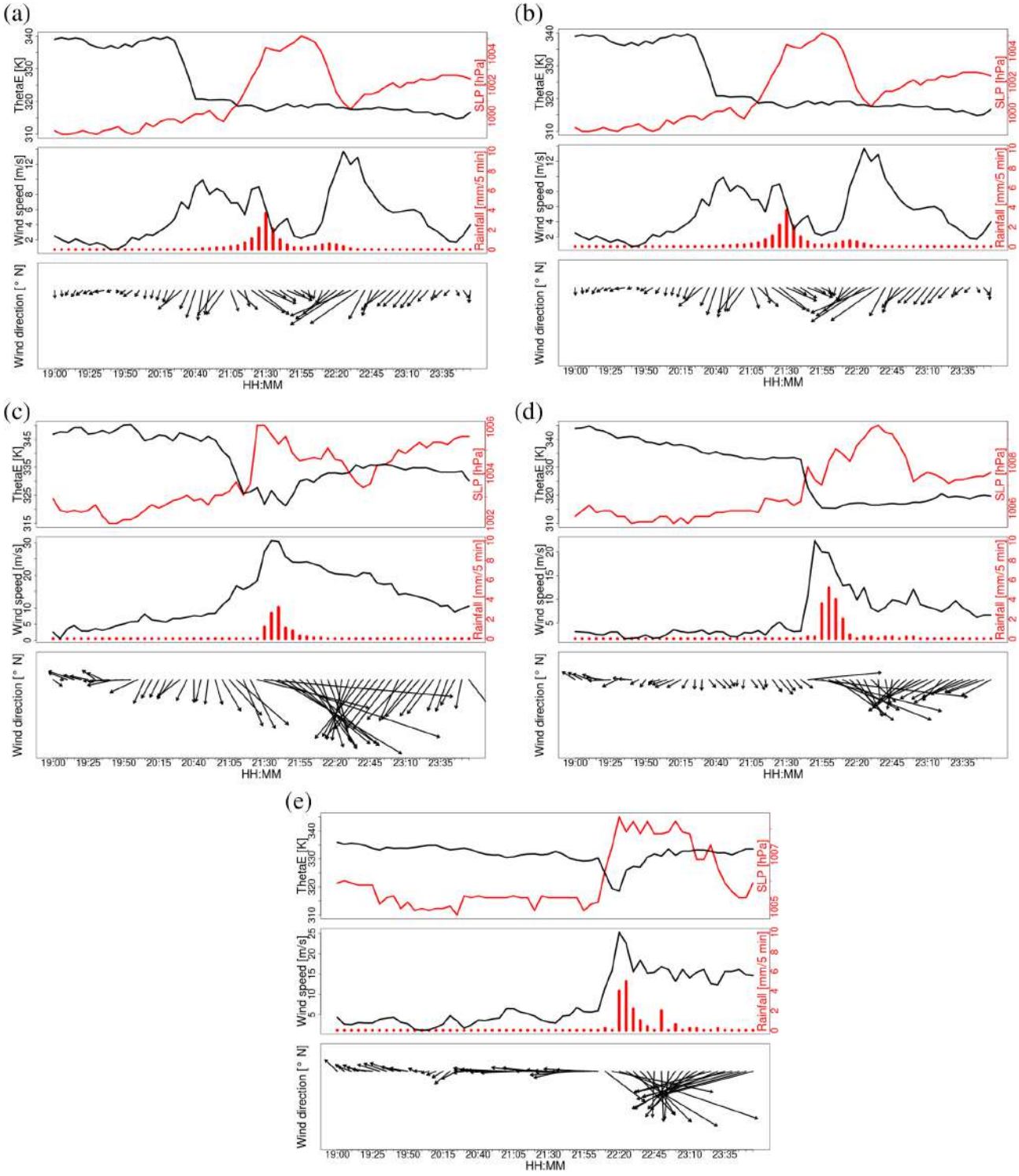

FIGURE 12 Time series of the meteorological stations at 5 min time step. The upper part shows the time series of equivalent potential temperature in black lines (unit of measure K, left axis), surface level pressure in red lines (unit of measure hPa, right axis). The centre part shows time series of wind velocity (unit of measure m s^{-1}) while the precipitation is represented in red bars (units mm $(5\ min)^{-1}$, right axis). The lower part shows the time series of wind direction and intensity in vectors. Stations are (a) Pala d'Altei, (b) Codroipo, (c) Lignano, (d) Fossalon, (e) Boa Paloma

gradually turning into northnortheasterly. The time lag between the decrease in temperature and the increase in pressure was smaller in Lignano than at the Codroipo station, suggesting either that the storm was moving faster or that the leading edge of the gust front was in closer proximity to the convective line near Lignano.

Nevertheless, some properties of gravity wave propagation were still present (change in winds, no change in temperature).

The Fossalon station (Figure 12d), located east of Lignano, shows a pressure rise at 2140 UTC associated with the drop in θ_e due to the gust front coming from the west (supported by the observed wind speed and direction), rather than the cold front from the north, while the following progressive pressure increase was associated with rain showers, constant θ_e and northerly to northeasterly winds.

Farther east, at the Boa Paloma buoy station, a relatively weak pressure rise occurred at 2150 UTC, just prior to the passage of the gust front (i.e. the typical pressure nose accompanying a well-structured gust front). The drop in θ_e was associated with a pressure drop, due to the increase in wind speed and divergence behind the gust front, that offsets the positive contribution to the pressure field from colder low-level air. Surface pressure increased significantly only after 2205 UTC, followed by the onset of weak precipitation (Figure 12e). The increase in pressure behind the leading edge of the gust front can be attributed to the non-hydrostatic pressure perturbation that develops in response to the diabatically cooled air (Wakimoto, 1982). East of Boa Paloma, the gust front perturbation cannot be identified in surface station time series and there are no VMI or Doppler images available after 2200 UTC, due to the radar auto-protection stop.

Another characteristic of bow echo storms, the rear inflow notch, is visible in the VMI, with a rear inflow jet in the Doppler velocity fields in the period 2125–2200 UTC (Figure 10b). Considering the Doppler range folding, speeds between 30 and 40 $m \cdot s^{-1}$ are estimated, in agreement with observed speeds at the surface stations. Note that the strongest gust, 45 $m \cdot s^{-1}$, was registered at Boa Paloma station at 2158 UTC, associated with the downdraft outflow. This station was in the path of the bow echo like storm core and shows a separation in time of about 15 min between the gust front (associated with the first pressure rise) and the cold pool (associated with the second, larger pressure rise).

The pre-squall meso-low overlaps with the gust front during the initial stage, due to the front inflow rising warm air from the pre-frontal environment into the core of the storm. Behind the convective line, the development of a meso-high is responsible for pressure rising, associated with the cold pool and rear inflow (details of the scheme of a mature squall system with internal features are shown in fig. 1 of Haertel and Johnson, 2000). After the onset of the northeasterly wind due to the synoptic pattern, again significant differences in θ_e arose between coastal and plain stations, marking the ending phase of the cold pool effects on the lower part of the local troposphere.

The analysis of different time steps within the evolution of the windstorm, performed by evaluating the time series of meteorological fields in the weather stations along the storm trajectory, shows that, in general, there are different relationships between pressure, wind and temperature. These varying relationships are due to the different dominating physical mechanisms for each stage of the storm. The early stage is characterized by synoptic forcing (cold front in Pala d'Altei); then there is a gravity wave propagation mechanism in Codroipo; after that, there is a synoptic/convective contribution in the middle (cold front and gravity current outflow in Lignano); lastly, there is a storm-scale convective contribution in the later stage (gust front dynamics in Fossalon and above all Boa Paloma). In the next section a simplified model is introduced to characterize the different phases of evolution better.

4 | DISCUSSION

4.1 | A simplified density current model

The temporal behaviour of the surface station parameters (wind, pressure and θ_e), measured in different surface stations, suggests that the observed high wind speed values are the result of different dynamic and thermodynamic forcing. The cold pool of the convective system, during its mature stage, is predicted to propagate at the speed of a density current, plus the advection of the synoptic wind. The higher propagation speed of the gust front, as seen in the Boa Paloma time series (Figure 12e), may be due to the wind surge associated with the rear inflow jet, which is proposed to be associated with the cold flow down the Alps.

In principle, the storm outflows are affected by both a non-hydrostatic and a hydrostatic contribution (Wakimoto, 1982; Haertel *et al*., 2001). It is considered that the horizontal pressure gradient due to the hydrostatic effect of the cold air is the main density current propagation mechanism (Moncrieff and Liu, 1999). The evaluation of such a gradient, using station data, allows an estimation of the forcing through a simplification of the x component of the horizontal momentum equation. The equation is given by:

$$\frac{\partial u}{\partial t} + u\frac{\partial u}{\partial x} + w\frac{\partial u}{\partial z} = -\frac{1}{\rho}\frac{\partial p}{\partial x} + \frac{\partial \tau_{xx}}{\partial x} + \frac{\partial \tau_{xz}}{\partial z} \qquad (1)$$

in which u is the horizontal downwind component (in a frame of reference having the x axis oriented in the direction of the storm movement), w is the vertical component of the wind, ρ is the density of the air mass, p is the pressure, and τ_{xx} and τ_{xz} are the horizontal and vertical shear stress terms. Note that the Coriolis term is neglected

because, in proximity of the ground, it is of a negligible order of magnitude compared to the other terms. An approximation of (1) can be made by considering a stationary flow in which w and the shear stress terms are negligible (Professor Matthew Parker, personal communication); these approximations reduce (1) to:

$$u\frac{\partial u}{\partial x} \approx -\frac{1}{\rho}\frac{\partial p}{\partial x} \tag{2}$$

After integration, the solution of (2) is:

$$\frac{u^2}{2} \approx \frac{\Delta p}{\rho} \tag{3}$$

or, rearranging,

$$u \approx \sqrt{2\frac{\Delta p}{\rho}} \tag{4}$$

where the Δp term is the pressure jump measured at a station at two consecutive times, representing two positions across the cold pool boundary. The density ρ was calculated using the ideal gas law by considering the different pressure and temperature values before, during and after the storm passage. The term indicated as Δp can be interpreted as the total finite pressure perturbation term, determined by the density current, so that the corresponding wind in (4) can be considered as the leading-edge density current wind.

Another estimation of the gust front leading-edge propagation speed can be derived from the VMI and Doppler images (Figure 10), when available. Considering the time of arrival of the pressure rise at Lignano and Boa Paloma stations, the speed of the system is approximately 15 $m \cdot s^{-1}$ (54 $km \cdot h^{-1}$). Comparing the observations of surface winds with the results from Equation (4), an estimation of the origin of the different components of the flow, associated with convective storms, can be made, keeping in mind that non-hydrostatic components, impacting the

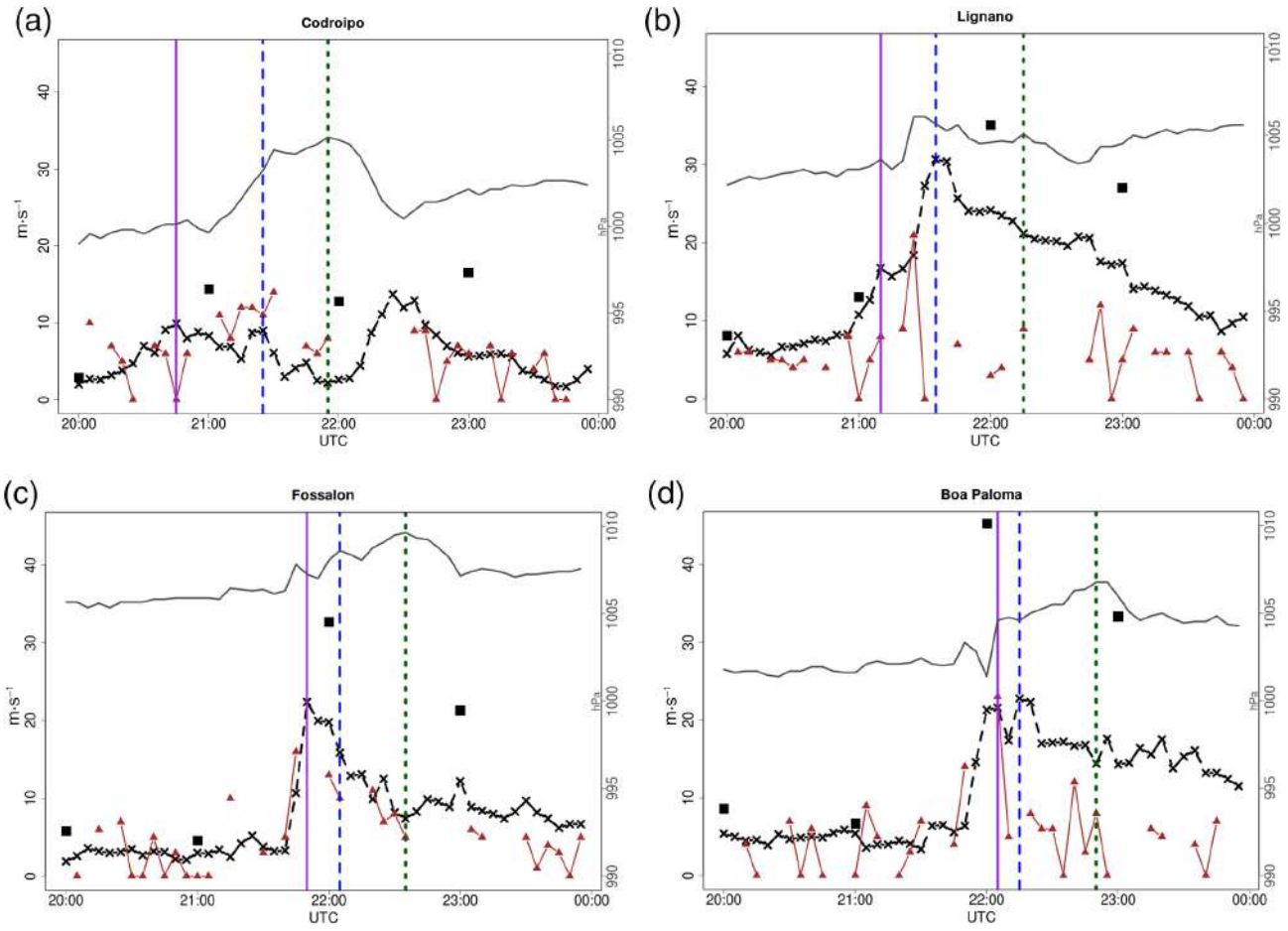

FIGURE 13 Time series of (a) Codroipo, (b) Lignano, (c) Fossalon and (d) Boa Paloma stations with expected values as obtained by the density current scheme. The thick line with crosses represents the 5 min wind; the black squares represent the gusts registered every hour; the thin grey line at the top represents the pressure (scale on the right); the triangles represent the estimation of wind according to Equation (4). The vertical lines represent different stages of storm: gust front (left), hydrostatic flow (centre), cold pool (right)

dynamics of the flows (Moncrieff and Liu, 1999; Haertel *et al.*, 2001), and ground friction are both neglected in this approach.

The time series of wind speed, measured at the surface stations and calculated based on (4), are reported in Figure 13 for all stations discussed in Section 3.4 except Pala d'Altei. The time series are from 2000 to 2400 UTC, August 8, 2008, as in Figure 12. Following Wakimoto (1982), three storm phases were identified and are marked in Figure 13: (1) the gust front phase (purple vertical line on the left), characterized by the arrival of the gust front measured at the station, as the observed maximum 5 min wind in the pre-storm phase; (2) the hydrostatic flow phase (blue dashed line in the centre), characterized by the observed 5 min wind immediately before the passage of the core of the storm precipitation, due to the hydrostatic pressure contribution to storm motion; (3) the cold pool phase (green dotted line on the right), characterized by the observed 5 min wind associated with the onset of measured precipitation (compare Figure 12 panels, associated with a relative maximum in pressure). These analyses provide insights into the times during which the storm movement could be attributed to a simple density current mechanism.

The wind speed calculated using Equation (4) (Figure 13, brown triangles) in general deviates from observations (Figure 13, black line). This may be due to the presence of non-hydrostatic flows, mixing in the proximity of thermodynamic boundaries (i.e. large gradients of θ_e) and local downdrafts/downbursts that can modify the speed predicted by this theory. Another reason for the discrepancy between the 5 min wind and the maximum gust can be ascribed to the propagation speed of the system (background flow), that affects the wind velocity relative to an observer at rest.

At Codroipo (Figure 13a), there was almost no change in wind speed in correspondence with the pressure rise near 2100 UTC following the gust front stage, indicating that neither the storm outflow nor the downslope wind flow from the mountains reached the surface at that stage. The convection was primarily organized along and supported by the cold front at this location. For this reason, the density current estimation of ground winds based on (4) should not be appropriate at this stage. Considering the hydrostatic and cold pool stages, the theory overestimates the wind in Codroipo, with values closer to the observed instantaneous gusts. As previously seen, following Haertel *et al.* (2001), a different mechanism, gravity wave propagation, theoretically explains this behaviour.

At Lignano (Figure 13b), the theoretical estimation of the gust front winds from (4) underestimates the speed, suggesting that there is also a relevant non-hydrostatic contribution. Pressure deviations associated with the passage of the storm are relatively small, since the storm had not reached its maximum strength yet (Wakimoto, 1982). Observed instantaneous wind gust values are similar to the 5 min wind. In that case, wind speeds are primarily dominated by the cold air advected from the mountains rather than by convective downdrafts (see also Figure 12).

The time series at Fossalon and Boa Paloma reflect the transition of a convective storm forced by a cold front to one supported by internal-dynamic storm processes. In fact, at Fossalon (Figure 13c) the theoretical and observed wind values are similar around the passage of the gust front, indicating that the storm motion is primarily controlled by internal density current processes rather than by the flow associated with the cold front. The following hydrostatic and cold pool stages are well matched by the model, but the strong fluctuations of pressure make computation of the derived wind very irregular.

Similar temporal evolutions are visible at Boa Paloma (Figure 13d), although the storm is deeper in the mature stage and the core is closer to this location. There is a more notable separation between the pressure rise associated with the gust front and that associated with the cold pool, typical of a mature stage convective system.

In this case the theoretical wind speed ahead of the gust front matches the observed 5 min wind. However, the gust front estimation matches the 5 min observed wind well, but largely underestimates the maximum gust (45 $m \cdot s^{-1}$), probably caused by the internal-storm process (rear inflow jet, diabatic cooling downdraft, shower drag) that became dominant at this stage of evolution. For classification purposes, Boa Paloma station measured a 45 $m \cdot s^{-1}$ maximum gust that agrees well with the results found in other bow echo cases (e.g. Atkins *et al.*, 2005), where the internal-storm dynamic dominates.

4.2 | A Froude number approach

Another approach to assess the role and contribution of wind blowing from the Alpine ridge can be based on Froude number analysis (Stein, 2004), due to the presence of an atmospheric flow impinging over an orographic ridge, whose behaviour can have consequences on the downhill side. For the cold front driven flow, an analysis can be performed by considering the Froude number, defined as:

$$F = \frac{u}{\sqrt{g' D}}, \tag{6}$$

where u is the wind velocity and g' is the reduced gravity acceleration defined as:

$$g' = g\left(\frac{\Delta\theta_e}{\theta_{e0}}\right)$$

θ_{e0} is the equivalent potential temperature of the pre-storm environment, $\Delta\theta_e$ is the change across the boundary and D is the depth of the advected flow or cold pool (Moncrieff and Liu, 1999). An estimation of D can be made according to Haertel *et al.* (2001), and references therein:

$$D = \frac{u^2}{k^2 g^*} \tag{7}$$

in which k is a parameter observed to be in the range 0.71–1.25 (but theoretical values for density currents are found to be approximately 1.4), g^* is calculated using the values of density derived from measurements before and after the storm passage at the stations, and u is the leading-edge velocity of the gust front, assumed to be in a steady state.

The estimated range of flow depth in (7) is 800–2,500 m, depending on k. Using these values in (6), with $\Delta\theta_e$ in the range 5–13 K, as measured at different surface stations, the results are that supercritical flow ($F > 1$) is obtained for a large region of the parameter space. The Froude number, computed for every station in Figure 12, shows that all values are supercritical except for Codroipo station, which has $F < 1$ for D above 1,500 m. The change from $F > 1$ to $F < 1$ indicates the transition from supercritical to subcritical flow, i.e. a hydraulic jump solution (Durran, 2003), associated with the displacement of the thunderstorms over topographic features (Frame and Markowski, 2006).

The hydraulic jump, seen in the Codroipo station time series (Figure 12b) around 2130 UTC, is associated with an increase in pressure, with minimal changes in surface wind and weak convective activity. This conclusion provides an explanation of the gravity wave hypothesis presented in Section 3.4 from a different perspective. The storm at that stage experienced an increase in intensity, followed by an increase in wind gusts at ground level. The hydraulic jump stage in the FVG plain marks the transition from externally driven storm forcing to internally driven storm forcing, as the gravity wave current advection mechanism overran the gravity wave propagation.

The objective analysis underlines the role of the cold front driven current as part of the mechanism that triggers/enhances the convective storm. Quantifying the role of this current as a rear inflow jet for the preexisting storm, and the subsequent intensification to a bow echo like system, would require a dedicated set of observations, specifically thermodynamic and kinematic information in the vertical transects along the storm, and is beyond the scope of the present study.

4.3 | A similar case

A recent work by Miglietta *et al.* (2016) studied a severe convective case in which two different convective cells, moving initially in parallel on the Veneto FVG plain, subsequently developed into two supercells which eventually merged, due to the right-hand movement of the northern cell (fig. 4d in Miglietta *et al.*, 2016). This merging caused a sort of "energy transfer" from the northern cell to the southern cell, since the former cell remained downwind with respect to the southeasterly low-level jet that was feeding the convection. A similar pattern can be observed in Figure 6b–d (in sequence), in which the southern cell is enhanced whereas the northern cell weakens just before merging.

This mechanism could be studied in more depth using high resolution simulations to understand better the implications in terms of severity and evolution of the storms and to assess their predictability.

5 | CONCLUSIONS

In this work, a severe convective storm producing severe winds and damage has been analysed. The storm impacted the Friuli Venezia Giulia (FVG) (northeastern Italy) plain and coastal region during the evening of August 8, 2008. The event was observed by means of surface data from a network of meteorological stations, radar reflectivity and velocity data from a C-band Doppler radar, enhanced RGB satellite images, lightning occurrences, and the ambient thermodynamic and kinematic conditions from radiosoundings. Different features were identified in the various stages of the storm lifetime, such as a bow echo like convective system, triggered by a cold front driven flow, that interacted with preexisting isolated convection enhancing its severity.

It is hypothesized that the rear inflow jet set up during the core stage of the storm has a larger scale guidance, other than the dynamic trigger internal to the convective cell core, as described in the literature (Weisman, 1993). This flow has been described as a density current (Haertel *et al.*, 2001) sloping down the Alps. A simple model based on an approximation of the horizontal momentum equation was used to calculate the expected values of the wind speed at the leading edge of the current. These values were compared to observations to discriminate the different contributions to the wind before, in proximity to and after the storm passage, at different ground stations. The results indicate that the measured winds are in good agreement with the density current simple model only in proximity to the coastal stations, while the model fails inland and at seaside stations,

and in general at the gust front stage of the storm. Hence, the major damage between Grado and Fossalon (camping Al Bosco) was very likely caused by convectively generated linear downbursts.

A further analysis of the cold front driven cold air was performed through Froude number estimation, which shows winds in a good agreement with the values expected for a supercritical flow. The results indicate the presence of a hydraulic jump as the flow transitions to subcritical at the base of the terrain; this could be associated with the southeastward movement and intensification of the convective system.

Such results are promising for a better understanding of the dynamics of severe weather occurrences that are observed in the FVG region, given that the event under analysis in the present study reached a considerable and highly impactful intensity along its path. Supplementary studies and different approaches can be achieved and are described in the following section.

5.1 | Future plans

Further analysis should be performed on the characteristics of the cold front density currents, such as climatology, thermodynamic analysis, statistical correlation between synoptically driven winds and convection occurrences. Additional work should be performed to understand the correlation between cold air moving down the slope of the Alps and enhanced convective activity over the plain and the coast of FVG. This could be explored by using specific instruments, like wind profilers, to describe the vertical evolution of the wind between the Prealps and the plain.

Another more comprehensive approach of approximating the density current speed (Dr Richard Rotunno, personal communication) is to consider the pressure equation for an incompressible fluid in a stationary state. This equation is derived by application of the divergence operator to Equation (1) in Section 4.1, in which thermodynamic (cold pool) and dynamic effects are taken into account as in the following equation:

$$\nabla^2 \mathrm{p} = -\nabla\cdot(\mathrm{u}\cdot\nabla\mathrm{u}) + \frac{\partial}{\partial z}\left(\frac{\mathrm{g}\cdot\theta'}{\theta_0}\right) + \nabla\cdot\left(\left(\frac{\partial\tau_{xx}}{\partial z}\right) + \left(\frac{\partial\tau_{xz}}{\partial z}\right)\right) \quad (5)$$

where the first term on the right-hand side is the dynamic downdraft effect, whereas the second term on the right-hand side is the thermodynamic cold pool effect (Equation (5) has the same variables as (1) except for θ' and θ_0, which are respectively the potential temperature perturbation and the potential temperature at a reference level and come from the vertical component of the momentum equation).

A solution can be found by decomposing the pressure into the components due to dynamic and effective buoyancy processes, as in Lombardo and Kading (2018); the proposed approach could be implemented in a future study based on fine-scale numerical simulations, required to gain more details.

Moreover, the Pala d'Altei station database could be an interesting source of information for such analysis, once the role of synoptic/mesoscale driven winds on downwind convection is assessed. Lastly, high resolution numerical simulations should be performed to understand and quantify the complex physical processes that support these types of events.

ACKNOWLEDGEMENTS

The authors want to thank many people and fellows who helped with this work: Professor Matthew Parker (North Carolina State University, USA) and Dr Richard Rotunno (NCAR, USA) for their valuable suggestions and Dr Martin Setvak (CHMI, Czech Republic) for Figure 8.

ORCID

Arturo Pucillo https://orcid.org/0000-0002-3709-4667

REFERENCES

Atkins, T.A., Przybylinski, R.W., Trapp, R.J. and Schmocker, G. (2005) Damaging surface wind mechanisms within the 10 June 2003 Sain Louis Bow Echo during BAMEX. *Monthly Weather Review*, 133, 2275–2296.

Bechini, R., Giaiotti, D., Manzato, A., Stel, F. and Micheletti, S. (2001) The June 4th 1999 severe weather episode in San Quirino, Italy: a tornado event? *Atmospheric Research*, 56, 213–232.

Bertato, M., Giaiotti, D., Manzato, A. and Stel, F. (2003) An interesting case of tornado in Friuli-Northeastern Italy. *Atmospheric Research*, 67-68, 3–21.

Bluestein, H.B. and Jain, M.H. (1985) Formation of mesoscale lines of precipitation: severe squall lines in Oklahoma during the Spring. *Journal of the Atmospheric Sciences*, 42, 1711–1732. https://doi.org10.1175/1520-0469(1985)042<1711:FOMLOP>2.0.CO;2.

Bolton, D. (1980) The computation of equivalent potential temperature. *Monthly Weather Review*, 108, 1046–1053.

Buzzi, A.S. and Tibaldi, S. (1978) Cyclogenesis in the lee of the Alps: a case study. *Quarterly Journal of the Royal Meteorological Society*, 104, 271–287.

Coniglio, M.C., Brooks, H.E., Weiss, S.J. and Corfidi, S.F. (2007) Forecasting the maintenance of quasi-linear mesoscale convective systems. *Weather Forecasting*, 22, 556–570. https://doi.org/10.1175/WAF1006.1.

Corbet, J.M., Mueller, C., Burghart, C., Gould, K. and Granger, G. (1994) ZEB: software for integration, display and management of diverse environmental datasets. *Bulletin of the American Meteorological Society*, 75, 783–792.

Davolio, S., Volonté, A., Manzato, A., Pucillo, A., Cicogna, A. and Ferrario, M.E. (2016) Mechanisms producing different

precipitation patterns over north-eastern Italy: insights from HyMeX-SOP1 and previous events. *Quarterly Journal of the Royal Meteorological Society*, 142, 188–205.

Durran, D.R. (2003) Downslope winds. In: Holton, J.R., Pyle, J. and Curry, J.A. (Eds.) *Encyclopedia of Atmospheric Sciences*. Seattle, WA: University of Washington. https://doi.org/10.1016/B0-12-227090-8/00288-8.

Feudale, L. and Manzato, A. (2014) Cloud-to-ground lightning distribution and its relationship with orography and anthropogenic emissions in the Po Valley. *Journal of Applied Meteorology and Climatology*, 53, 2651–2670.

Frame, J. and Markowski, P. (2006) The interaction of simulated squall lines with idealized mountain ridges. *Monthly Weather Review*, 134, 1919–1941.

French, A.J. and Parker, M.D. (2014) Numerical simulations of bow echo formation following a squall line–supercell merger. *Monthly Weather Review*, 142, 4791–4822.

George, H. and Knievel, J.C. (2006) *What is a bow echo? Symposium on the Challenges of Severe Convective Storms, January 27 – February 3* 2006, Atlanta GA: American Meteorological Society.

Giaiotti, D., Gianesini, E. and Stel, F. (2001) Heuristic considerations pertaining to hailstone size distributions in the plain of Friuli Venezia Giulia. *Atmospheric Research*, 57, 269–288.

Giaiotti, D., Giovannoni, M., Pucillo, A. and Stel, F. (2007) The climatology of tornadoes and waterspouts in Italy. *Atmospheric Research*, 83, 534–541.

Haertel, P.T. and Johnson, R.H. (2000) The liner dynamics of squall line mesohighs and wake lows. *Journal of the Atmospheric Sciences*, 57, 93–107.

Haertel, P.T., Johnson, R.H. and Tulich, S.N. (2001) Some simple simulations of thunderstorm outflows. *Journal of the Atmospheric Sciences*, 58, 504–516.

Isotta, F.A., Frei, C., Weilguni, V., Perčec Tadić, M., Lassegues, P., Rudolf, B., Pavan, V., Cacciamani, C., Antolini, G., Ratto, S. M., Munari, M., Micheletti, S., Bonati, V., Lussana, C., Ronchi, C., Panettieri, E., Marigo, G. and Vertačnik, G. (2014) The climate of daily precipitation in the Alps: development and analysis of a high-resolution grid dataset from pan-Alpine rain-gauge data. *International Journal of Climatology*, 34, 1657–1675.

Lombardo, K.A. and Colle, B.A. (2010) The spatial and temporal distribution of organized convective structures over the northeast and their ambient conditions. *Monthly Weather Review*, 138, 4456–4474. https://doi.org/10.1175/2010MWR3463.1.

Lombardo, K. and Colle, B.A. (2012) Ambient conditions associated with the maintenance and decay of quasi-linear convective systems crossing the northeastern U.S. coast. *Monthly Weather Review*, 140, 3805–3819.

Lombardo, K. and Kading, T. (2018) The behavior of squall lines in horizontally heterogeneous coastal environments. *Journal of the Atmospheric Sciences*, 75, 1243–1269. https://doi.org/10.1175/JAS-D-17-0248.1, in press.

Manzato, A. and Morgan, G.M., Jr. (2003) Evaluating the sounding instability with the Lifted Parcel Theory. *Atmospheric Research*, 67-68, 455–473.

Manzato, A. (2007) The 6 hours climatology of thunderstorms and rainfalls in the Friuli Venezia Giulia plain. *Atmospheric Research*, 83, 336–348. https://doi.org/10.1016/j.atmosres.2005.08.013.

Manzato, A. (2012) Hail in northeast Italy: climatology and bivariate analysis with the sounding-derived indices. *JAMC*, 51, 449–466.

Manzato, A., Davolio, S., Miglietta, M.M., Pucillo, A. and Setvak, M. (2015) 12 September 2012: a supercell outbreak in NE Italy? *Atmospheric Research*, 153, 98–118.

McGinley, J. (1982) A diagnosis of Alpine lee cyclogenesis. *Monthly Weather Review*, 110, 1271–1287.

Miglietta, M.M., Manzato, A. and Rotunno, R. (2016) Characteristics and predictability of a supercell during HyMeX SOP1. *Quarterly Journal of the Royal Meteorological Society*, 142, 2839–2853.

Miglietta, M.M., Mazon, J., Motola, V. and Pasini, A. (2017) Effect of positive sea surface temperature anomaly on a Mediterranean tornadic supercell. *Scientific Reports*, 7, 12828.

Miglietta, M.M., Arai, K., Kusunoki, K., Inoue, H., Adachi, T. and Niino, H. (2019) Automatic detection of vortices using OPERA Doppler radar data: an application to a waterspout in northern Italy. *Atmospheric Research*. (in press).

Moncrieff, M.W. and Liu, C. (1999) Convection initiation by density currents: role of convergence, shear, and dynamical organization. *Monthly Weather Review*, 127, 2455–2464.

Morgan, G.M., Jr. (1992) ThetaPlot, an equivalent potential temperature diagram. *Meteorology and Atmospheric Physics*, 47, 259–265.

Parker, M.D. and Johnson, R.H. (2000) Organizational modes of midlatitude mesoscale convective systems. *Monthly Weather Review*, 128, 3413–3436.

Pavan, V., Antolini, G., Barbiero, R., Berni, N., Brunier, F., Cacciamani, C., Cagnati, A., Czzuli, O., Cicogna, A., De Luigi, C., Di Carlo, E., Francioni, M., Maraldo, L. and Marigo, G. (2019) High resolution climate precipitation analysis for north-central Italy, 1961–2015. *Climate Dynamics*, 52, 3435–3453. https://doi.org/10.1007/s00382-018-4337-6.

Poelman, D.R., Schulz, W., Diendorfer, G. and Bernardi, M. (2016) The European lightning location system EUCLID – Part 2: Observations. *Natural Hazards and Earth System Sciences*, 16, 607–616.

Pucillo, A., Giaiotti, D. and Stel, F. (2009) Ground wind convergence as source of deep convection. *Atmospheric Research*, 93, 437–445.

Pucillo, A. and Manzato, A. (2013) Usefulness and skill of station-derived predictors in the forecasting storm occurrence and intensity. *Atmospheric Research*, 123, 31–47.

Stein, J. (2004) Exploration of some convective regimes over the Alpine orography. *Quarterly Journal of the Royal Meteorological Society*, 130, 481–502.

Steinacker, R. (1984) Airmass and frontal movement around the Alps. *Rivista di Meteorologia Aeronautica*, 43, 85–93.

Taszarek, M., Allen, J., Pùčik, T., Groenemeijer, P., Czernecki, B., Kolendowicz, L., Lagouvardos, K., Kotroni, V. and Schulz, W. (2019a) A climatology of thunderstorms across Europe from a synthesis of multiple data sources. *Journal of Climate*, 32, 1813–1837.

Taszarek, M., Pilguj, N., Orlikowski, J., Surowiecki, A., Walczakiewicze, A., Pilorzf, W., Piaseckid, K., Pajurekg, Ł. and Półrolniczaka, M. (2019b) Derecho evolving from a mesocyclone—a study of 11 August 2017 severe weather outbreak in Poland: event analysis and high-resolution simulation. *Monthly Weather Review*, 147, 2283–2306.

Wakimoto, R.M. (1982) The life cycle of thunderstorm gust fronts as viewed with Doppler radar and rawinsonde data. *Monthly Weather Review*, 110, 1060–1082.

Wakimoto, R.M., Murphey, H.V., Davis, C.A. and Atkins, N.T. (2006) High winds generated by bow echoes. Part II: The relationship between the mesovortices and damaging straight-line winds. *Monthly Weather Review*, 134, 2813–2829.

Weisman, M.L. (1993) The genesis of severe, long-lived bow echoes. *Journal of the Atmospheric Sciences*, 50, 645–670. https://doi.org/10.1175/1520-0469(1993)050<0645:TGOSLL>2.0.CO;2.

How to cite this article: Pucillo A, Miglietta MM, Lombardo K, Manzato A. Application of a simple analytical model to severe winds produced by a bow echo like storm in northeast Italy. *Meteorol Appl*. 2020;27:e1868. https://doi.org/10.1002/met.1868